Letters

Modeling and Stability Assessment of Single-Phase Grid Synchronization Techniques: Linear Time-Periodic Versus Linear Time-Invariant Frameworks

Saeed Golestan, *Senior Member, IEEE*, Josep M. Guerrero, *Fellow, IEEE*, and Juan C. Vasquez, *Senior Member, IEEE*

***Abstract*—The grid synchronization unit, which is often based on a phase-locked loop (PLL) or a frequency-locked loop (FLL), highly affects the power converter performance and stability, particularly under weak grid conditions. It implies that a careful stability assessment of grid synchronization techniques (GSTs) is of vital importance. This task is most often based on obtaining a linear time-invariant (LTI) model for the GST and applying standard stability tests to it. Another option is modeling and dynamics/stability assessment of GSTs in the linear time-periodic (LTP) framework, which has received a little attention. In this letter, the procedure of deriving the LTP model for single-phase GSTs is first demonstrated. The accuracy of the LTP model in predicting the GST dynamic behavior and stability is then evaluated and compared with that of the LTI one. Two well-known single-phase GSTs, i.e., the second-order generalized integrator-based FLL (SOGI-FLL) and enhanced PLL (EPLL), are considered as the case studies.**

***Index Terms*—Frequency-locked loop (FLL), generalized inverse Nyquist stability criterion, harmonic transfer function, linear time-periodic (LTP) systems, modeling, phase-locked loop (PLL), single-phase systems, stability analysis, synchronization.**

I. Introduction

RECENT developments in the technology of semiconductor and signal processing have made power electronic converters more efficient and cost-effective than before [1]. These converters are now widely utilized for interfacing renewable energy-based sources, particularly wind and photovoltaic systems, and electric vehicles with the grid [2]. They are also fundamental components in building equipment such as uninterruptible power supplies, active filters, electric motor drives, etc. Depending on the application in hand, grid-connected power converters may have different topologies and control structures [3]–[5]. But, almost all of them have something in common: they require a synchronization unit. This part is mainly responsible for coordinating the power converter output and the grid voltage so that they can safely and efficiently work in parallel. There are different ways of implementing this unit. A common practice is to use a phase-locked loop (PLL) [6]–[8] or a frequency-locked loop (FLL) [9]–[12] for this purpose.

Manuscript received March 19, 2018; revised April 6, 2018; accepted April 15, 2018. Date of publication May 9, 2018; date of current version November 19, 2018. *(Corresponding author: Saeed Golestan.)*

The authors are with the Department of Energy Technology, Aalborg University, Aalborg DK-9220, Denmark (e-mail:

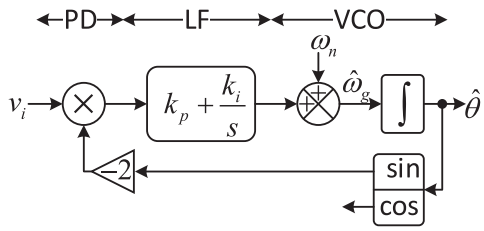

Fig. 1. Block diagram of the pPLL. v_i is the grid voltage signal, ω_n is the nominal frequency, $\hat{\theta}$ and $\hat{\omega}_g$ are the estimated phase angle and frequency, respectively, and k_i and k_p are the integral and proportional gains of the proportional-integral (PI) controller, respectively.

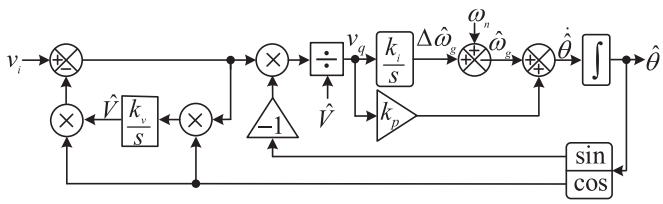

Fig. 2. Block diagram of the EPLL. $\hat{V}$ is the estimated amplitude and k_v is the gain of the amplitude estimation loop. Other parameters have been defined before in the caption of Fig. 1. Throughout this manuscript, it is assumed that $k_v = k_p$.

PLLs are nonlinear feedback control systems with three distinct elements: phase detector (PD), loop filter (LF), and voltage-controlled oscillator (VCO) [13]. Fig. 1 illustrates a standard single-phase PLL, often called the power-based PLL (pPLL), in which these parts are highlighted [14]. This standard PLL, however, suffers from large double-frequency oscillatory ripples in its output signals [14], [15]. Solving this problem has been the main motivation behind developing more advanced single-phase PLLs [7]. For example, in [16], an enhanced PLL (EPLL) is proposed to deal with the pPLL double-frequency problem. The EPLL, which its block diagram is shown in Fig. 2, has been designed using an optimization procedure. The complete elimination of the aforementioned double-frequency oscillations in the steady state, estimating the grid voltage amplitude that makes the amplitude normalization possible, and achieving a higher

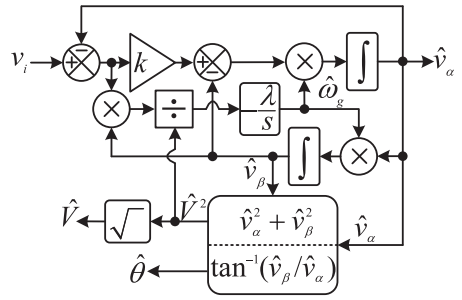

Fig. 3. Block diagram of the SOGI-FLL. k and λ are the SOGI-FLL parameters, and $\hat{v}_\alpha$ and $\hat{v}_\beta$ are estimations of the fundamental component of the grid voltage and its quadrature version, respectively. Other parameters have been already defined in the captions of Figs. 1 and 2.

filtering ability and a more smooth transient performance in detecting the grid voltage frequency[1] while maintaining the implementation simplicity are the main features of the EPLL. A review of other advanced single-phase PLLs can be found in [7].

FLLs are also like PLLs have a nonlinear closed-loop nature, but they are (most often) implemented in the stationary frame. Designing FLLs may be carried out in different ways. In single-phase applications, which are the focus of this letter, they are often constructed using a second-order generalized integrator (SOGI). Fig. 3 illustrates a SOGI-FLL, which is a standard single-phase FLL [10]. This structure includes a SOGI in a unity feedback control loop and a frequency estimation algorithm for adjusting the SOGI resonance frequency. The SOGI outputs are estimations of the grid voltage fundamental component and its quadrature version, which are used for estimating the grid voltage amplitude and phase.

The dynamics/stability assessment of the grid synchronization technique (GST) is very important as it is a crucial element in the control of single-phase grid-connected power converters and significantly affects their performance. This task is most often carried out by deriving a linear time-invariant (LTI) model for the GST [14], [17]. Another option is the linear time-periodic (LTP) modeling and the stability analysis in the LTP framework, which have received a little attention for the study of GSTs.

The key feature of an LTP model is taking into account the coupling between different frequencies, which results from periodic dynamics in the system [18], [19]. These dynamics may be caused by the underlying physics of the system or its control requirements. The rotating machines (e.g., helicopters and wind power plants) and multirate systems are well-known systems that their dynamics can be described by an LTP model [18]. For other examples, see [20]–[23].

The main aim of this letter is demonstrating the procedure of deriving LTP models for single-phase GSTs and evaluating the accuracy of these models in predicting the GST stability and dynamic behavior compared to the LTI models. The EPLL and SOGI-FLL are considered as the case studies here. The main reason behind selecting the EPLL is that a large number of single-phase PLLs are mathematically equivalent to it or have a close relationship with it [24]. The SOGI-FLL is also the basic structure for designing a large number of single-phase FLLs [25]–[28].

[1]It is because of tapping the estimated frequency from the PI regulator integrator output instead of the VCO input.

II. Modeling

A. SOGI-FLL

1) LTP Modeling: Before presenting the LTP modeling of the SOGI-FLL, it should be mentioned that this procedure has some similarities with the SOGI-FLL LTI modeling, which has been presented before in [17] and [28].

To derive the SOGI-FLL LTP model, some assumptions need to be made. First, it is assumed that the single-phase input signal of the SOGI-FLL is as

$$v_i = V\cos(\theta) \tag{1}$$

where V and θ are the amplitude and phase angle of this signal, respectively. It is also assumed that the $\alpha\beta$-axis outputs of the SOGI-FLL, which are estimations of the input signal fundamental component and its quadrature version, are as

$$\hat{v}_\alpha = \hat{V}\cos(\hat{\theta}) \tag{2}$$

$$\hat{v}_\beta = \hat{V}\sin(\hat{\theta}) \tag{3}$$

where $\hat{V}$ and $\hat{\theta}$ are estimations of the amplitude and phase angle of the SOGI-FLL input signal, respectively, and may be expressed as

$$\hat{\theta} = \tan^{-1}(\hat{v}_\beta/\hat{v}_\alpha) \tag{4}$$

$$\hat{V} = \sqrt{\hat{v}_\beta^2+\hat{v}_\alpha^2}. \tag{5}$$

The following differential equations may also be easily obtained from the SOGI-FLL structure (Fig. 3):

$$\dot{\hat{\omega}}_g = -\frac{\lambda}{\hat{V}^2}\hat{v}_\beta(v_i-\hat{v}_\alpha) \tag{6}$$

$$\dot{\hat{v}}_\alpha = \hat{\omega}_g(kv_i - k\hat{v}_\alpha - \hat{v}_\beta) \tag{7}$$

$$\dot{\hat{v}}_\beta = \hat{\omega}_g\hat{v}_\alpha. \tag{8}$$

The time differentiation of (4) is equal to

$$\dot{\hat{\theta}} = \frac{\dot{\hat{v}}_\beta\hat{v}_\alpha - \dot{\hat{v}}_\alpha\hat{v}_\beta}{\hat{v}_\alpha^2+\hat{v}_\beta^2}. \tag{9}$$

Substituting (7) and (8) into (9) gives

$$\begin{aligned}\dot{\hat{\theta}} &= \frac{\hat{\omega}_g\left(\hat{v}_\alpha^2+\hat{v}_\beta^2\right) - k\hat{\omega}_g\hat{v}_\beta(v_i-\hat{v}_\alpha)}{\hat{v}_\alpha^2+\hat{v}_\beta^2}\\ &= \hat{\omega}_g - \frac{k\hat{\omega}_g\hat{v}_\beta(v_i-\hat{v}_\alpha)}{\hat{v}_\alpha^2+\hat{v}_\beta^2}.\end{aligned} \tag{10}$$

By considering (5) and (6), (10) can be rewritten as

$$\dot{\hat{\theta}} = \hat{\omega}_g + \frac{k\hat{\omega}_g}{\lambda}\dot{\hat{\omega}}_g. \tag{11}$$

Defining $\hat{\theta} = \theta_n + \Delta\hat{\theta}$ and $\hat{\omega}_g = \omega_n + \Delta\hat{\omega}_g$, where Δ denotes a small perturbation and $\theta_n = \int \omega_n\,dt$, and substituting them

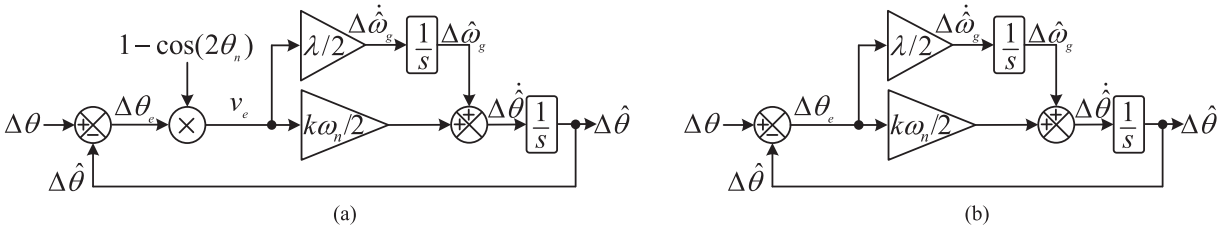

Fig. 4. Block diagram representation of the SOGI-FLL linear models. (a) The LTP model. (b) The LTI model. Without loss of generality, it can be assumed that $\theta_n = \omega_n t$.

into (11) results in

$$\dot{\theta}_n + \Delta\dot{\hat{\theta}} = \omega_n + \Delta\hat{\omega}_g + \frac{k\left(\omega_n + \Delta\hat{\omega}_g\right)}{\lambda}\Delta\dot{\hat{\omega}}_g. \tag{12}$$

Considering that $\dot{\theta}_n = \omega_n$ and assuming that the product $\Delta\hat{\omega}_g\Delta\dot{\hat{\omega}}_g$ is negligible, (12) can be simplified as

$$\Delta\dot{\hat{\theta}} \approx \Delta\hat{\omega}_g + \frac{k\omega_n}{\lambda}\Delta\dot{\hat{\omega}}_g. \tag{13}$$

Equation (13) depends on the time differentiation of $\Delta\hat{\omega}_g$. Therefore, to obtain a complete LTP model, we need a linear differential equation for describing the dynamics of the frequency estimation.

By substituting (1)–(3) into (6), we have

$$\begin{aligned}\Delta\dot{\hat{\omega}}_g &= -\frac{\lambda}{\hat{V}^2}\hat{V}\sin\left(\hat{\theta}\right)\left(V\cos\left(\theta\right) - \hat{V}\cos\left(\hat{\theta}\right)\right)\\ &= \frac{\lambda}{2\hat{V}}\left(V\sin\left(\theta-\hat{\theta}\right) - \boldsymbol{V\sin\left(\theta+\hat{\theta}\right) + \hat{V}\sin\left(2\hat{\theta}\right)}\right).\end{aligned} \tag{14}$$

Considering the definitions $\hat{\theta} = \theta_n + \Delta\hat{\theta}$ and $\hat{\omega}_g = \omega_n + \Delta\hat{\omega}_g$, which were presented before, and defining $\theta = \theta_n + \Delta\theta$ and assuming that $V \approx \hat{V}$, (14) can be simplified as

$$\begin{aligned}\Delta\dot{\hat{\omega}}_g \approx \frac{\lambda}{2}\Big(&\sin\left(\Delta\theta - \Delta\hat{\theta}\right) - \sin\left(2\theta_n + \Delta\theta + \Delta\hat{\theta}\right)\\ &+ \sin\left(2\theta_n + 2\Delta\hat{\theta}\right)\Big).\end{aligned} \tag{15}$$

Using trigonometric identities, (15) can be rewritten as

$$\begin{aligned}\Delta\dot{\hat{\omega}}_g \approx \frac{\lambda}{2}\Big(&\overbrace{\sin\left(\Delta\theta - \Delta\hat{\theta}\right)}^{\approx(\Delta\theta-\Delta\hat{\theta})}\\ &- \cos\left(2\theta_n\right)\overbrace{\left[\sin\left(\Delta\theta + \Delta\hat{\theta}\right) - \sin\left(2\Delta\hat{\theta}\right)\right]}^{\approx(\Delta\theta-\Delta\hat{\theta})}\\ &+ \sin\left(2\theta_n\right)\overbrace{\left[\cos\left(2\Delta\hat{\theta}\right) - \cos\left(\Delta\theta + \Delta\hat{\theta}\right)\right]}^{\approx 0}\Big)\\ \approx \frac{\lambda}{2}&\underbrace{\left\{1-\cos\left(2\theta_n\right)\right\}\left(\Delta\theta - \Delta\hat{\theta}\right)}_{v_e}.\end{aligned} \tag{16}$$

Using (13) and (16), the linear state-space model of the SOGI-FLL can be obtained as

$$\begin{aligned}\underbrace{\begin{bmatrix}\Delta\dot{\hat{\omega}}_g\\ \Delta\dot{\hat{\theta}}\end{bmatrix}}_{\dot{\boldsymbol{x}}} &\approx \underbrace{\begin{bmatrix}0 & -\frac{\lambda}{2}\left\{1-\cos\left(2\theta_n\right)\right\}\\ 1-\frac{k\omega_n}{2}\left\{1-\cos\left(2\theta_n\right)\right\} & \end{bmatrix}}_{\boldsymbol{A}}\underbrace{\begin{bmatrix}\Delta\hat{\omega}_g\\ \Delta\hat{\theta}\end{bmatrix}}_{\boldsymbol{x}}\\ &\quad+\underbrace{\begin{bmatrix}\frac{\lambda}{2}\left\{1-\cos\left(2\theta_n\right)\right\}\\ \frac{k\omega_n}{2}\left\{1-\cos\left(2\theta_n\right)\right\}\end{bmatrix}}_{\boldsymbol{B}}\Delta\theta\\ y &= \underbrace{\begin{bmatrix}0 & 1\end{bmatrix}}_{\boldsymbol{C}}\begin{bmatrix}\Delta\hat{\omega}_g\\ \Delta\hat{\theta}\end{bmatrix}\end{aligned} \tag{17}$$

in which $\boldsymbol{x}$ denotes the state vector. Notice that matrices $\boldsymbol{A}$ and $\boldsymbol{B}$ in (17) are time-periodic with a period equal to $T_n/2$ because $A(t+T_n/2) = A(t)$ and $B(t+T_n/2) = B(t)$ ($T_n = 2\pi/\omega_n$ is the nominal grid fundamental period). Therefore, (17) describes an LTP system. The block diagram representation of (17) is shown in Fig. 4(a).

In this stage, it may be interesting to briefly talk about the SOGI-FLL LTI model and its difference compared to the LTP one. For deriving the SOGI-FLL LTI model, equations (1)–(14) are still valid [17]. Nevertheless, it is assumed that the double-frequency (highlighted) terms in (14) cancel each other. This assumption results in

$$\Delta\dot{\hat{\omega}}_g \approx \frac{\lambda V}{2\hat{V}}\sin\left(\theta - \hat{\theta}\right) \tag{18}$$

which can be approximated by

$$\Delta\dot{\hat{\omega}}_g \approx \frac{\lambda}{2}(\Delta\theta - \Delta\hat{\theta}). \tag{19}$$

Using (13) and (19), the LTI state-space model of the SOGI-FLL and its block diagram representation can be obtained as expressed in (20) and as shown in Fig. 4(b) [17].

$$\begin{aligned}\underbrace{\begin{bmatrix}\Delta\dot{\hat{\omega}}_g\\ \Delta\dot{\hat{\theta}}\end{bmatrix}}_{\dot{\boldsymbol{x}}} &\approx \underbrace{\begin{bmatrix}0 & -\frac{\lambda}{2}\\ 1-\frac{k\omega_n}{2} & \end{bmatrix}}_{\boldsymbol{A}}\underbrace{\begin{bmatrix}\Delta\hat{\omega}_g\\ \Delta\hat{\theta}\end{bmatrix}}_{\boldsymbol{x}} + \underbrace{\begin{bmatrix}\frac{\lambda}{2}\\ \frac{k\omega_n}{2}\end{bmatrix}}_{\boldsymbol{B}}\Delta\theta\\ y &= \underbrace{\begin{bmatrix}0 & 1\end{bmatrix}}_{\boldsymbol{C}}\begin{bmatrix}\Delta\hat{\omega}_g\\ \Delta\hat{\theta}\end{bmatrix}.\end{aligned} \tag{20}$$

It can be observed that the trigonometric term $\cos\left(2\theta_n\right)$ does not appear in the LTI model. This is the only difference of the LTI and LTP models of the SOGI-FLL.

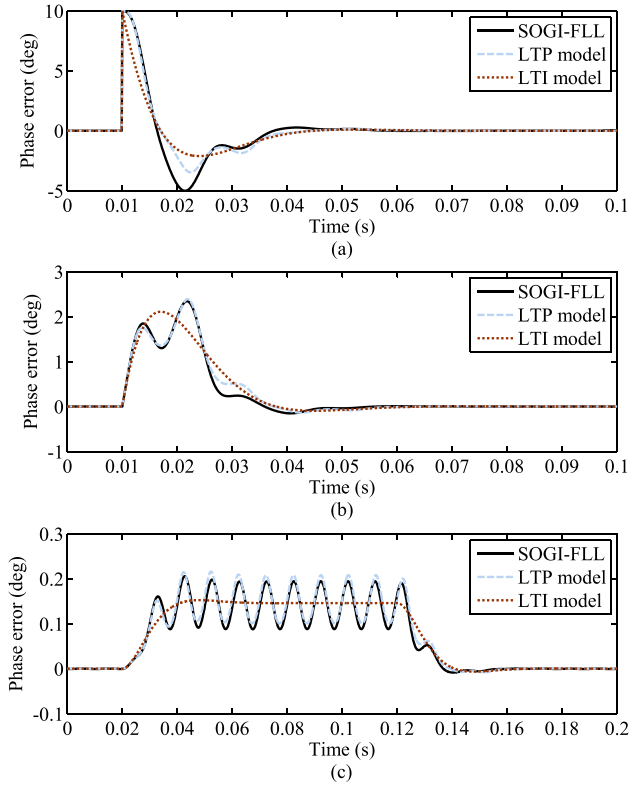

Fig. 5. Performance of the SOGI-FLL and its LTP and LTI models in response to the following tests. (a) Test 1. (b) Test 2. (3) Test 3. Control parameters: $k = \sqrt{2}$ and $\lambda = 49\,348$.

2) Accuracy Comparison of LTP and LTI Models: The aim of this section is performing a comparison between the LTP and LTI models in predicting the SOGI-FLL dynamic behavior. To this end, the performance of the actual SOGI-FLL and its LTP and LTI models in response to the following three tests are compared:

Test 1: A 10° phase angle jump happens.
Test 2: A 2 Hz frequency jump occurs.
Test 3: A 10 Hz/s frequency ramping for a period of 0.1 s happens.

The SOGI-FLL control parameters in this study are $k = \sqrt{2}$ and $\lambda = 49\,348$. These parameters have been designed in [17]. The amplitude and the nominal frequency of the SOGI-FLL input signal are considered to be 1 p.u. and 50 Hz, respectively. The sampling frequency is fixed at 10 kHz. The third-order integrator method is used for the discretization of the SOGI [29].

Fig. 5 illustrates the results of the SOGI-FLL and its LTP and LTI models in response to the aforementioned tests. For the sake of brevity, only the phase error response is shown. The LTI model, as shown, only predicts the SOGI-FLL average behavior. The LTP model, however, offers a higher accuracy and even can predict the double-frequency oscillations of the SOGI-FLL transient response.

B. EPLL

1) LTP Modeling: By considering (1) as the EPLL input signal, the signal v_q in the EPLL structure (Fig. 2) can be expressed as

$$\begin{aligned} v_q = \frac{\Delta\dot{\hat{\omega}}_g}{k_i} &= -\frac{1}{\hat{V}}\left(V\cos(\theta) - \hat{V}\cos(\hat{\theta})\right)\sin(\hat{\theta}) \\ &= \frac{1}{2\hat{V}}\left(V\sin(\theta-\hat{\theta}) - \boldsymbol{V\sin(\hat{\theta}+\theta) + \hat{V}\sin(2\hat{\theta})}\right). \end{aligned} \tag{21}$$

Regardless of a simple coefficient, this equation is the same as (14). Therefore, following the same assumptions and definitions made immediately after (14), it can be approximated by

$$\begin{aligned} v_q = \frac{\Delta\dot{\hat{\omega}}_g}{k_i} &\approx \frac{1}{2}\Big(\sin(\Delta\theta - \Delta\hat{\theta}) - \sin(2\theta_n + \Delta\theta + \Delta\hat{\theta}) \\ &\qquad + \sin(2\theta_n + 2\Delta\hat{\theta})\Big) \\ &\approx \frac{1}{2}\underbrace{\{1-\cos(2\theta_n)\}(\Delta\theta - \Delta\hat{\theta})}_{v_e}. \end{aligned} \tag{22}$$

From the EPLL structure (Fig. 2), we have

$$\dot{\hat{\theta}} = \hat{\omega}_g + k_p v_q \tag{23}$$

or equivalently

$$\Delta\dot{\hat{\theta}} = \Delta\hat{\omega}_g + k_p v_q. \tag{24}$$

Based on (22) and (24), the LTP state-space model of the EPLL and its block diagram representation can be obtained as expressed in (25) and as shown in Fig. 6(a).

$$\begin{aligned} \underbrace{\begin{bmatrix} \Delta\dot{\hat{\omega}}_g \\ \Delta\dot{\hat{\theta}} \end{bmatrix}}_{\dot{\boldsymbol{x}}} &\approx \underbrace{\begin{bmatrix} 0 & -\frac{k_i}{2}\{1-\cos(2\theta_n)\} \\ 1 & -\frac{k_p}{2}\{1-\cos(2\theta_n)\} \end{bmatrix}}_{\boldsymbol{A}} \underbrace{\begin{bmatrix} \Delta\hat{\omega}_g \\ \Delta\hat{\theta} \end{bmatrix}}_{\boldsymbol{x}} \\ &\quad + \underbrace{\begin{bmatrix} \frac{k_i}{2}\{1-\cos(2\theta_n)\} \\ \frac{k_p}{2}\{1-\cos(2\theta_n)\} \end{bmatrix}}_{\boldsymbol{B}} \Delta\theta \\ y &= \underbrace{\begin{bmatrix} 0 & 1 \end{bmatrix}}_{\boldsymbol{C}} \begin{bmatrix} \Delta\hat{\omega}_g \\ \Delta\hat{\theta} \end{bmatrix}. \end{aligned} \tag{25}$$

Notice that this model is the same as the SOGI-FLL model if $k_i = \lambda$ and $k_p = k\omega_n$. Based on this fact, we can conclude that, from the small-signal point of view, the SOGI-FLL is the stationary frame equivalent of the EPLL. This equivalence has also been pointed out in [30].

The block diagram representation of the LTI model of the EPLL may also be observed in Fig. 6(b). This model can be obtained by assuming that the highlighted (double-frequency) terms in (21) cancel each other. We had the same discussion before for the case of the SOGI-FLL. Therefore, to save the space, it is not repeated here.

2) Accuracy Comparison of LTP and LTI Models: For the accuracy assessment of the LTP and LTI models of the EPLL, the same conditions and tests as those described in Section II-A2 are considered. Fig. 7 demonstrates the results of this assessment. Similar to the SOGI-FLL case, it is seen that the LTI model

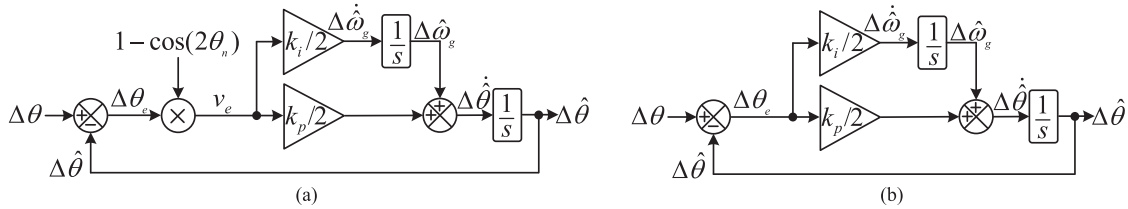

Fig. 6. Block diagram representation of the EPLL linear models. (a) LTP model. (b) LTI model.

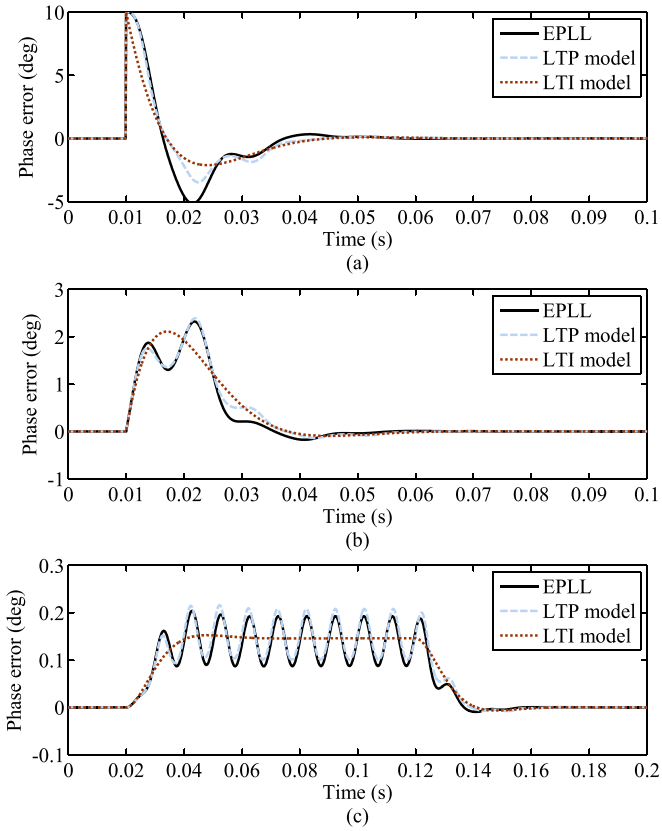

Fig. 7. Performance of the EPLL and its LTP and LTI models in response to the following tests. (a) Test 1. (b) Test 2. (3) Test 3. Control parameters: $k_p = k_v = 444$ and $k_i = 49\,348$.

just predicts the EPLL average behavior. The LTP model, however, provides a higher accuracy because it can even predict the double-frequency oscillations during the transient response of the EPLL. Comparing the EPLL results in these tests with those of the SOGI-FLL (see Fig. 5) also further supports the equivalence of these two structures.

III. Stability Analysis

As the SOGI-FLL and EPLL are mathematically equivalent, we only focus on one of them, SOGI-FLL, in this section.

A. Stability Analysis Using LTI Model

The LTI systems benefit from a frequency separation characteristic, which means that a signal with a particular frequency in their input results in a signal with the same frequency (possibly with a different amplitude and initial phase angle) in their output in the steady state. Therefore, open-loop and closed-loop transfer functions of the LTI systems may be readily obtained, which make their analysis and design easy. For the case of SOGI-FLL, these transfer functions can be obtained from Fig. 4(b) as follows:

$$G_{ol}^{LTI}(s) = \frac{\Delta\hat{\theta}(s)}{\Delta\theta_e(s)} = \frac{(k\omega_n/2)\,s + (\lambda/2)}{s^2} = K\frac{\overbrace{s+\omega_z}^{G(s)}}{s^2} \tag{26}$$

$$G_{cl}^{LTI}(s) = \frac{\Delta\hat{\theta}(s)}{\Delta\theta(s)} = \frac{(k\omega_n/2)\,s + (\lambda/2)}{s^2 + (k\omega_n/2)\,s + (\lambda/2)} = \frac{K(s+\omega_z)}{s^2 + Ks + K\omega_z}. \tag{27}$$

where $K = k\omega_n/2$ and $\omega_z = \lambda/(k\omega_n)$.

From (27), it can be observed that the characteristic polynomial is second-order. According to the Routh–Hurwitz criterion, both roots of this polynomial are in the left half plane if $k > 0$ and $\lambda > 0$ (or, equivalently, $K > 0$ and $\omega_z > 0$). As this condition always holds, the LTI model predicts that the SOGI-FLL is an unconditionally stable system.

B. Stability Analysis Using LTP Model

In LTP systems, contrary to LTI ones, injecting a single frequency component in their input leads to multiple frequency components in their output [31]. Consequently, there exists a coupling between different frequencies in the input and output of the LTP system, which makes its transfer function representation elusive. To deal with this problem, the concept of the harmonic transfer function (HTF) has been proposed, which represents an LTP system as an infinite-dimensional LTI system [18]. In what follows, the open-loop HTF of the SOGI-FLL is obtained.

Based on the SOGI-FLL LTP model [Fig. 4(a)], the signal v_e can be expressed as a function of the phase error signal $\Delta\theta_e$ as follows:

$$v_e(t) = (1 - \cos(2\theta_n))\,\Delta\theta_e(t) \tag{28}$$

where as mentioned before, $\theta_n = \omega_n t$. According to Euler's formula and defining $\omega_p = 2\omega_n$, (28) can be rewritten as

$$v_e(t) = -\frac{1}{2}e^{j\omega_p t}\Delta\theta_e(t) + \Delta\theta_e(t) - \frac{1}{2}e^{-j\omega_p t}\Delta\theta_e(t) \tag{29}$$

or equivalently in the Laplace domain as

$$v_e(s) = -\frac{1}{2}\Delta\theta_e(s - j\omega_p) + \Delta\theta_e(s) - \frac{1}{2}\Delta\theta_e(s + j\omega_p). \tag{30}$$

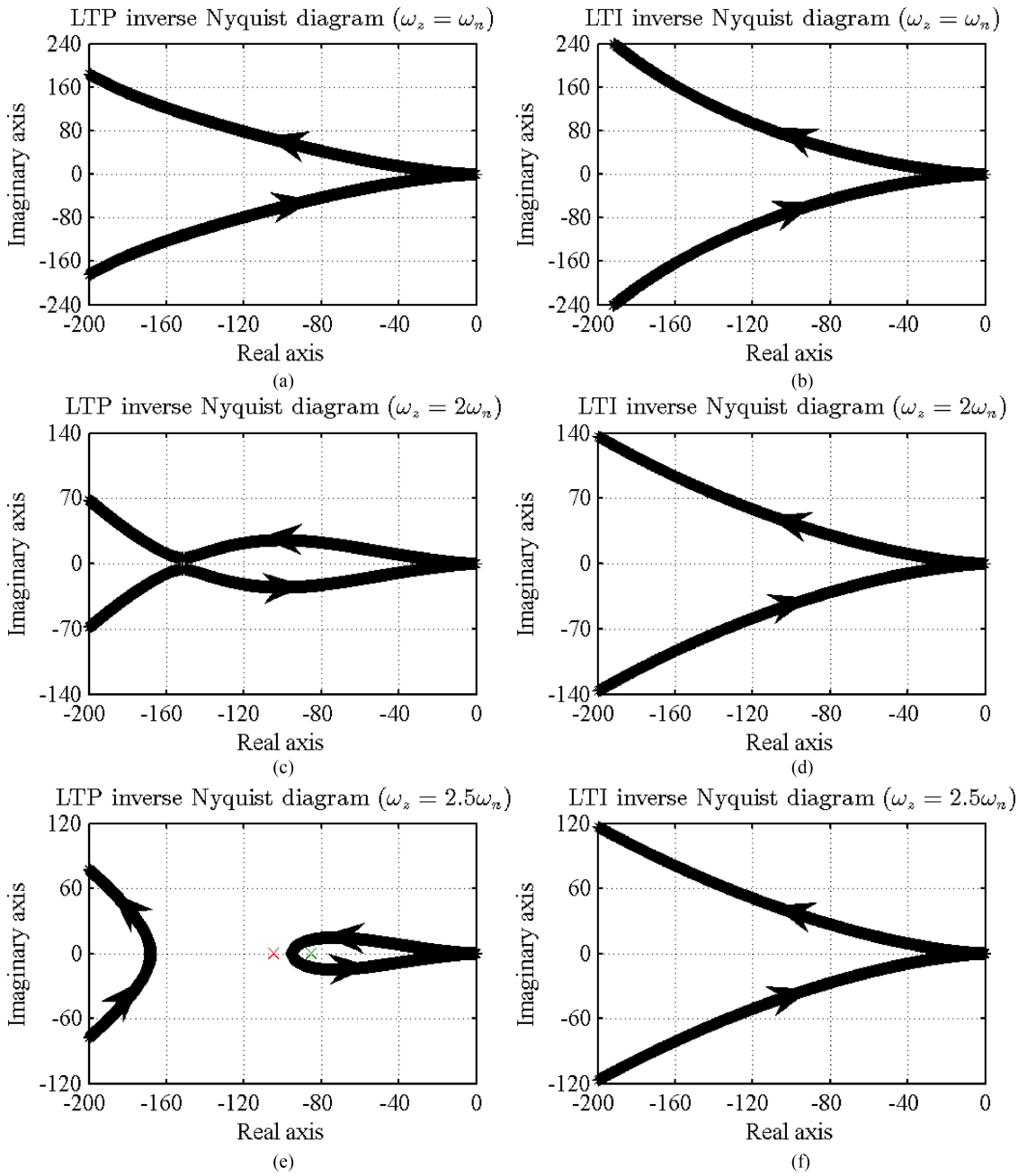

Fig. 8. Inverse Nyquist diagrams of the SOGI-FLL LTI and LTP models.

Using (30) and Fig. 4(a), the output of the LTP model of the SOGI-FLL can be expressed as

$$\Delta\hat{\theta}(s) = \underbrace{\frac{(k\omega_n/2)\,s + \lambda/2}{s^2}}_{KG(s)} v_e(s)$$

$$= KG(s)\left[-\frac{1}{2}\Delta\theta_e(s - j\omega_p) + \Delta\theta_e(s) - \frac{1}{2}\Delta\theta_e(s + j\omega_p)\right]. \tag{31}$$

Substituting s by $s + jm\omega_p$, where $m \in \mathbb{Z}$, in both sides of (31) gives

$$\Delta\hat{\theta}(s + jm\omega_p) = K\overbrace{G(s + jm\omega_p)}^{G_m(s)}\left[-\frac{1}{2}\Delta\theta_e(s + j(m-1)\omega_p) + \Delta\theta_e(s + jm\omega_p) - \frac{1}{2}\Delta\theta_e(s + j(m+1)\omega_p)\right]. \tag{32}$$

Using (32), the open-loop HTF of the SOGI-FLL can be obtained as expressed in (33) shown at the bottom of the next page. It can be observed that this HTF is a doubly infinite matrix. Therefore, to perform the stability analysis, we have no choice but to use a truncated version of it. Notice that the truncated

HTF should be symmetrical, i.e., it should include the same number of positive and negative harmonics.

As we are dealing with a multi-input multi-output (MIMO) system here, and interested to analyze the stability of the closed-loop system for any $K > 0$, the generalized Nyquist stability criterion is applied [32], [33]. Notice that, because of the LTP system folding effect, eigenloci of the truncated open-loop HTF is plotted for $-j0.5\omega_p \leq s \leq +j0.5\omega_p$ [34]. Notice also that $\omega_p = 2\omega_n$.

Fig. 8(a) illustrates the LTP inverse Nyquist diagram[2] of $\mathcal{G}$ [see (33)] for $\omega_z = \omega_n$. As a reference for comparison, the inverse Nyquist diagram of the LTI transfer function $G(s)$ [see (26)] for the same value of ω_z is shown in Fig. 8(b). Both diagrams predict that the SOGI-FLL remains stable for positive values of K, which are corresponding to all points on the negative real axis. By increasing the value of ω_z, some ripples appear in the LTP inverse Nyquist diagram [see Fig. 8(c)]. The LTI one, however, does not predict them [see Fig. 8(d)]. When ω_z becomes larger than $\omega_p = 2\omega_n$, the LTP inverse Nyquist diagram makes a symmetrical circuit on the negative real axis [see Fig. 8(e)]. Notice that the net encirclements of the real-axis points surrounded by this circuit are equal to zero. It means that these points result in a stable operation for the SOGI-FLL, and the real points outside this circuit and enclosed by the outer one makes the SOGI-FLL unstable.

To verify this prediction, $K = 85$ and $\omega_z = 2.5\omega_n$ are selected as the initial values of the SOGI-FLL parameters. The value of K is suddenly increased to 105. Notice that, as highlighted in Fig. 8(e), the real-axis points -85 and -105 are inside and outside the circuit, respectively. Fig. 9 illustrates the SOGI-FLL performance in response to this test. This result has been obtained using a dSPACE platform with a sampling frequency of 10 kHz. As correctly predicted by the LTP inverse Nyquist diagram, this increase of K makes the SOGI-FLL unstable. The LTI inverse Nyquist diagram, however, incorrectly predicts that the SOGI-FLL should remain stable [see Fig. 8(f)]. The SOGI-FLL will be stable again by reducing K to its original value. To save the space, this result is not shown.

[2]Here, the inverse Nyquist diagrams make the interpretation easier than the Nyquist plots. Therefore, they are chosen for the representation.

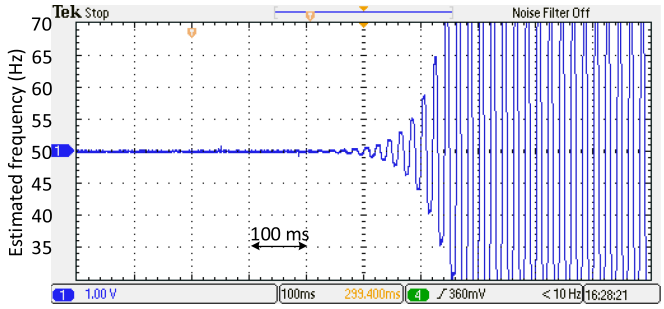

Fig. 9. SOGI-FLL performance when a sudden change in its control parameters is applied. The initial parameters are $K = 85$ and $\omega_z = 2.5\omega_n$. After change, they are $K = 105$ and $\omega_z = 2.5\omega_n$.

IV. Discussion and Conclusion

The LTP modeling of two well-known single-phase synchronization techniques, i.e., the SOGI-FLL and EPLL, was presented here. It was shown using simulation results that the LTP model, contrary to the LTI one which can only predict the average dynamic behavior of the synchronization techniques, may even predict the double-frequency oscillations in their transient response. By developing the open-loop HTF and applying the generalized inverse Nyquist stability criterion, it was also demonstrated that these synchronization techniques (contrary to the LTI model prediction) may become unstable.

Admittedly, the aforementioned instability may only happen because of a poor selection of the control parameters. It, however, implies that the LTI models are not completely perfect in predicting the stability of single-phase synchronization techniques. Indeed, the LTP ones offer a higher accuracy in this regard. Therefore, to ensure the stability of single-phase synchronization techniques, we recommend developing and considering both the LTI and LTP models during their analysis/design procedure. This is particularly important for the advanced synchronization techniques. Notice that these techniques often include different kinds of low-pass/band-pass/notch filters and multiple feedback loops in their structures and, therefore, are more prone to the instability.

$$\begin{bmatrix} \vdots \\ \Delta\hat{\theta}(s-j2\omega_p) \\ \Delta\hat{\theta}(s-j\omega_p) \\ \Delta\hat{\theta}(s) \\ \Delta\hat{\theta}(s+j\omega_p) \\ \Delta\hat{\theta}(s+j2\omega_p) \\ \vdots \end{bmatrix} = K \underbrace{\begin{bmatrix} \ddots & \vdots & \vdots & \vdots & \vdots & \vdots & \iddots \\ \cdots & G_{-2}(s) & -0.5G_{-2}(s) & 0 & 0 & 0 & \cdots \\ \cdots & -0.5G_{-1}(s) & G_{-1}(s) & -0.5G_{-1}(s) & 0 & 0 & \cdots \\ \cdots & 0 & -0.5G_0(s) & G_0(s) & -0.5G_0(s) & 0 & \cdots \\ \cdots & 0 & 0 & -0.5G_{+1}(s) & G_{+1}(s) & -0.5G_{+1}(s) & \cdots \\ \cdots & 0 & 0 & 0 & -0.5G_{+2}(s) & G_{+2}(s) & \cdots \\ \iddots & \vdots & \vdots & \vdots & \vdots & \vdots & \ddots \end{bmatrix}}_{\mathcal{G}} \begin{bmatrix} \vdots \\ \Delta\theta_e(s-j2\omega_p) \\ \Delta\theta_e(s-j\omega_p) \\ \Delta\theta_e(s) \\ \Delta\theta_e(s+j\omega_p) \\ \Delta\theta_e(s+j2\omega_p) \\ \vdots \end{bmatrix} \tag{33}$$

REFERENCES

[1] H. Wang, M. Liserre, and F. Blaabjerg, "Toward reliable power electronics: Challenges, design tools, and opportunities," *IEEE Ind. Electron. Mag.*, vol. 7, no. 2, pp. 17–26, Jun. 2013.

[2] M. Liserre, T. Sauter, and J. Y. Hung, "Future energy systems: Integrating renewable energy sources into the smart power grid through industrial electronics," *IEEE Ind. Electron. Mag.*, vol. 4, no. 1, pp. 18–37, Mar. 2010.

[3] M. Rivera *et al.*, "Review of predictive control methods to improve the input current of an indirect matrix converter," *IET Power Electron.*, vol. 7, no. 4, pp. 886–894, Apr. 2014.

[4] F. Blaabjerg, R. Teodorescu, M. Liserre, and A. V. Timbus, "Overview of control and grid synchronization for distributed power generation systems," *IEEE Trans. Ind. Electron.*, vol. 53, no. 5, pp. 1398–1409, Oct. 2006.

[5] S. Kouro, J. I. Leon, D. Vinnikov, and L. G. Franquelo, "Grid-connected photovoltaic systems: An overview of recent research and emerging PV converter technology," *IEEE Ind. Electron. Mag.*, vol. 9, no. 1, pp. 47–61, Mar. 2015.

[6] S. Golestan, J. M. Guerrero, and J. C. Vasquez, "Three-phase PLLs: A review of recent advances," *IEEE Trans. Power Electron.*, vol. 32, no. 3, pp. 1894–1907, Mar. 2017.

[7] S. Golestan, J. M. Guerrero, and J. C. Vasquez, "Single-phase PLLs: A review of recent advances," *IEEE Trans. Power Electron.*, vol. 32, no. 12, pp. 9013–9030, Dec. 2017.

[8] M. Karimi-Ghartemani, *Enhanced Phase-locked Loop Structures for Power and Energy Applications*. Hoboken, NJ: Wiley, 2014.

[9] X. He, H. Geng, and G. Yang, "A generalized design framework of notch filter based frequency-locked loop for three-phase grid voltage," *IEEE Trans. Ind. Electron.*, vol. 65, no. 9, pp. 7072–7084, Sep. 2018.

[10] P. Rodriguez, A. Luna, I. Candela, R. Mujal, R. Teodorescu, and F. Blaabjerg, "Multiresonant frequency-locked loop for grid synchronization of power converters under distorted grid conditions," *IEEE Trans. Ind. Electron.*, vol. 58, no. 1, pp. 127–138, Jan. 2011.

[11] S. Golestan, J. M. Guerrero, J. Vasquez, A. M. Abusorrah, and Y. A. Al-Turki, "A study on three-phase FLLs," *IEEE Trans. Power Electron.*, to be published.

[12] P. Rodriguez, A. Luna, R. S. Munoz-Aguilar, I. Etxeberria-Otadui, R. Teodorescu, and F. Blaabjerg, "A stationary reference frame grid synchronization system for three-phase grid-connected power converters under adverse grid conditions," *IEEE Trans. Power Electron.*, vol. 27, no. 1, pp. 99–112, Jan. 2012.

[13] F. M. Gardner, *Phaselock Techniques*. Hoboken, NJ: Wiley, 2005.

[14] R. M. S. Filho, P. F. Seixas, P. C. Cortizo, L. A. B. Torres, and A. F. Souza, "Comparison of three single-phase PLL algorithms for UPS applications," *IEEE Trans. Ind. Electron.*, vol. 55, no. 8, pp. 2923–2932, Aug. 2008.

[15] T. Thacker, D. Boroyevich, R. Burgos, and F. Wang, "Phase-locked loop noise reduction via phase detector implementation for single-phase systems," *IEEE Trans. Ind. Electron.*, vol. 58, no. 6, pp. 2482–2490, Jun. 2011.

[16] M. Karimi-Ghartemani and M. R. Iravani, "A method for synchronization of power electronic converters in polluted and variable-frequency environments," *IEEE Trans. Power Syst.*, vol. 19, no. 3, pp. 1263–1270, Aug. 2004.

[17] S. Golestan, E. Ebrahimzadeh, J. M. Guerrero, and J. C. Vasquez, "An adaptive resonant regulator for single-phase grid-tied VSCs," *IEEE Trans. Power Electron.*, vol. 33, no. 3, pp. 1867–1873, Mar. 2018.

[18] N. M. Wereley, "Analysis and control of linear periodically time varying systems," Ph.D. dissertation, Department of Aeronautics and Astronautics, Massachusetts Institute of Technology, 1990.

[19] E. Möllerstedt, "Dynamic analysis of harmonics in electrical systems," Ph.D. dissertation, Department of Automatic Control, Lund Institute of Technology, 2000.

[20] J. R. C. Orillaza and A. R. Wood, "Harmonic state-space model of a controlled TCR," *IEEE Trans. Power Del.*, vol. 28, no. 1, pp. 197–205, Jan. 2013.

[21] R. Z. Scapini, L. V. Bellinaso, and L. Michels, "Stability analysis of AC-DC full-bridge converters with reduced DC-link capacitance," *IEEE Trans. Power Electron.*, vol. 33, no. 1, pp. 899–908, Jan. 2018.

[22] N. R. Chaudhuri, R. Oliveira, and A. Yazdani, "Stability analysis of vector-controlled modular multilevel converters in linear time-periodic framework," *IEEE Trans. Power Electron.*, vol. 31, no. 7, pp. 5255–5269, Jul. 2016.

[23] V. Salis, A. Costabeber, S. M. Cox, A. Formentini, and P. Zanchetta, "Stability assessment of high-bandwidth DC voltage controllers in single-phase active-front-ends: LTI vs LTP models," *IEEE J. Emerg. Sel. Topics Power Electron.*, to be published.

[24] M. Karimi-Ghartemani, "A unifying approach to single-phase synchronous reference frame PLLs," *IEEE Trans. Power Electron.*, vol. 28, no. 10, pp. 4550–4556, Oct. 2013.

[25] Z. Xin, X. Wang, Z. Qin, M. Lu, P. C. Loh, and F. Blaabjerg, "An improved second-order generalized integrator based quadrature signal generator," *IEEE Trans. Power Electron.*, vol. 31, no. 12, pp. 8068–8073, Dec. 2016.

[26] Z. Xin, R. Zhao, P. Mattavelli, P. C. Loh, and F. Blaabjerg, "Reinvestigation of generalized integrator based filters from a first-order-system perspective," *IEEE Access*, vol. 4, pp. 7131–7144, 2016.

[27] J. Matas, M. Castilla, J. Miret, L. G. de Vicuna, and R. Guzman, "An adaptive prefiltering method to improve the speed/accuracy tradeoff of voltage sequence detection methods under adverse grid conditions," *IEEE Trans. Ind. Electron.*, vol. 61, no. 5, pp. 2139–2151, May 2014.

[28] S. Golestan, J. M. G. GE, J. Vasquez, A. M. Abusorrah, and Y. A. Al-Turki, "Modeling, tuning, and performance comparison of second-order generalized integrator-based FLLs," *IEEE Trans. Power Electron.*, to be published.

[29] M. Ciobotaru, R. Teodorescu, and F. Blaabjerg, "A new single-phase PLL structure based on second order generalized integrator," in *Proc. 37th IEEE Power Electron. Spec. Conf.*, Jun. 2006, pp. 1–6.

[30] M. K. Ghartemani, S. A. Khajehoddin, P. K. Jain, and A. Bakhshai, "Problems of startup and phase jumps in PLL systems," *IEEE Trans. Power Electron.*, vol. 27, no. 4, pp. 1830–1838, Apr. 2012.

[31] N. M. Wereley and S. R. Hall, "Linear time periodic systems: Transfer function, poles, transmission zeroes and directional properties," in *Proc. Am. Control Conf.*, Jun. 1991, pp. 1179–1184.

[32] J. F. Barmanj and J. Katzenelson, "A generalized Nyquist-type stability criterion for multivariable feedback systems," *Int. J. Contr.*, vol. 20, no. 4, pp. 593–622, 1974.

[33] A. G. MacFarlane and I. Postlethwaite, "The generalized Nyquist stability criterion and multivariable root loci," *Int. J. Contr.*, vol. 25, no. 1, pp. 81–127, 1977.

[34] S. R. Hall and N. M. Wereley, "Generalized Nyquist stability criterion for linear time periodic systems," in *Proc. Am. Control Conf.*, May 1990, pp. 1518–1525.